Waste Disposal & Sustainable Energy (2022) 4:149–155
https://doi.org/10.1007/s42768-022-00095-2

ARTICLE

Ar-plasma enhanced copper-nickel alloy catalysis for ammonia synthesis

Zhou Yimeng[1] · **Lv Jiabao**[1] · **Peng Yaqi**[1] · **Lin Xiaoqing**[1] · **Lv Xingjie**[1] · **Ye Qiulin**[1] · **Liu Shaojun**[1] · **Wu Angjian**[1] · **Li Xiaodong**[1]

Received: 15 March 2022 / Revised: 30 March 2022 / Accepted: 3 April 2022 / Published online: 17 May 2022

Abstract

Ammonia (NH_3) synthesis via electrocatalytic nitrogen reduction generally suffers from low NH_3 yield and faradaic efficiency. Compared with activating stable, low-solubility N_2, the electrochemical conversion of nitrates to ammonia provides a more reasonable route for NH_3 production. Herein, we introduce Ar-plasma to enhance the interaction between copper-nickel alloys and carbon substrate to improve the performance of NH_3 production. The NH_3 faradaic efficiency from nitrate is nearly 100% and the yield rate is over 6000 $\mu g_{NH_3} cm^{-2} h^{-1}$. DFT (density functional theory) calculation reveals the high performance of $Cu_{50}Ni_{50}$ originates from the lower energy barrier on the reaction path and the closer position to the Fermi level of the d-band center. This work offers a promising strategy for plasma-modified electrocatalyst to promote ammonia synthesis via nitrate reduction.

Keywords Ammonia synthesis · Plasma modification · Nitrate conversion · Copper-nickel alloy

Introduction

NH_3 is one of the largest chemicals in the world and is industrially produced through the Haber–Bosch process (HBP). However, this method uses high-purity hydrogen as a raw material and requires harsh catalytic conditions (450–500 °C, 20–30 MPa), consuming 1%–2% of the global energy supply and emitting more than 1% of carbon dioxide simultaneously [1–3]. The strict reaction conditions and high energy cost from HBP are attributed to the high dissociation energy of the N≡N bond of N_2 molecules (941 kJ mol^{-1}) [4–6]. Recently, nitrate was proposed as a promising nitrogen source with a relatively low dissociation energy (204 kJ mol^{-1}) and better reaction kinetics for NH_3 synthesis. In fact, NO_3^- induced by human activities has increased over time and is commonly regarded as a notorious waste or hazardous pollutant [7, 8]. With the inherent advantages of high aqueous solubility and easy activation of the N=O bond, the difficulty related to direct nitrogen conversion can be well addressed. At the same time, this strategy will alleviate the environmental issue, i.e., reducing the risks of methemoglobinemia and various types of cancers caused by the uptake of nitrates from daily life [9–11]. Nevertheless, the competing hydrogen evolution reaction is also of concern in the electrocatalytic nitrate reduction process. Hydrogen can occupy the active sites on the surface of the electrocatalysts, which affects the adsorption of nitrate. Therefore, a reasonable design of catalysts and electrolysis system is essential to realize efficient electrocatalytic nitrate reduction for NH_3 production [12, 13].

Dima et al. studied the cyclic voltammograms of several precious metals in nitrate reduction, which indicated that Cu exhibited a higher current density and better electrocatalytic performance [14]. McEnaney et al. found that high concentrations of protons and nitrate ions are essential to achiev high selectivity. Under the conditions of −1 V (vs. RHE (reversible hydrogen electrode)) and NH_3 partial current density of −22 mA cm^{-2}, the faradaic efficiency reached a peak of 82% [15]. Wang et al. proved enhanced NO_3^- reduction performance on $Cu_{50}Ni_{50}$ alloy catalysts, including a 0.12 V upshift in the half-wave potential and

---

Peng Yaqi
pengyaqi@zju.edu.cn

Li Xiaodong
lixd@zju.edu.cn

[1] State Key Laboratory of Clean Energy Utilization, Department of Energy Engineering, Zhejiang University, Hangzhou 310028, China

a sixfold increase in activity compared to those obtained with pure Cu at 0 V (vs. RHE) [16]. Fu et al. applied copper nanosheets as an electrocatalyst to reduce nitrates, achieving a current density of 10 mA cm^{-2} at a low overpotential of −0.15 V. The ammonia formation rate of Cu nanosheets was 390.1 $\mu g_{NH_3} cm^{-2} h^{-1}$ with the highest faradaic efficiency reaching 99.7% [17].

In this work, we proposed a strategy to improve the NH_3 yield and faradaic efficiency of the nitrate-to-NH_3 reaction by enhancing the interaction between the substrate and catalysts via Ar-plasma. A series of CuNi alloys with different Cu/Ni ratios were investigated in terms of their electrocatalytic activity. Through Ar-plasma modification, the faradaic efficiency was enhanced by 57% at −0.27 V (vs. RHE) with an NH_3 yield rate of 4293 $\mu g_{NH_3} cm^{-2} h^{-1}$. DFT (density functional theory) calculations were performed to reveal the origin of the electrocatalytic activity. Eventually, in situ FTIR (Fourier-transform infrared) spectroscopy was performed to investigate the effect of Ar-plasma modification on the substrate. Based on this study, an effective strategy to improve the electrosynthesis of NH_3 is anticipated.

Materials and methods

Catalyst synthesis

The catalysts used in this work were prepared via electrodeposition in a typical three-electrode cell with a carbon substrate as the working electrode, and a Pt electrode and an Ag/AgCl electrode (with 3 mol L^{-1} KCl) were used as the counter electrode and reference electrode, respectively. 0.05 mol L^{-1} H_2SO_4 mixed with 20 mol L^{-1} $CuSO_4 + NiSO_4$ solutions were used as the deposition baths. The Cu/Ni ratio of the synthesized catalysts was controlled by adjusting the ratio of $CuSO_4/NiSO_4$. Carbon paper (SGL Carbon, Wiesbaden, Germany) was used as a substrate and current collector. After constant-current operation at 200 mA cm^{-2} at ambient temperature for 5 min, CuNi on a carbon substrate was obtained. The as-prepared electrodes of the Cu/Ni alloy were rinsed with deionized water and then dried in a N_2 atmosphere overnight for subsequent electrocatalysis. Herein, the electrocatalyst CuNi alloys were labeled $Cu_{80}Ni_{20}$, $Cu_{50}Ni_{50,}$ and $Cu_{30}Ni_{70}$ according to the Cu/Ni ratios set in the deposition solutions, which were 80/20, 50/50, and 30/70, respectively. To enhance the adhesion between the electrocatalyst and carbon substrate, inductively coupled plasma (ICP) was used to treat the pristine substrate using a 13.56 MHz power source (OTF-1200X, Kejing, Hefei, China). The as-prepared carbon substrate was treated with plasma in a homemade reactor. The reactor was first evacuated at a pressure of approximately 2 Pa before the plasma gas was introduced. Then, the carbon substrate was treated with Ar-plasma for 5 min with a flow rate of 25 mL min^{-1} and the plasma power of 300 W.

Material characterization and NH_3 synthesis evaluation

The morphology of the synthesized catalysts before and after Ar-plasma modification was investigated by scanning electron microscopy (SEM) (Hitachi SU-8010, Hitachi, Tokyo, Japan) and transmission electron microscopy (TEM) (Hitachi HT-7700, Hitachi, Tokyo, Japan). The crystal structures of the samples were characterized via X-ray diffraction (XRD) with the D/max-2550 diffractometer (Rigaku, Tokyo, Japan) at room temperature. Atomic force microscopy (AFM, Dimension Icon, Bruker Nano INC, Berlin, Germany) was used to estimate the roughness change of the carbon substrate induced by plasma treatment. In situ FTIR spectroscopy was performed using a Nicolet iS50 (Thermo Fisher, Waltham, MA, USA) equipped with a mercury cadmium telluride detector. The reference spectrum was collected at −0.8 V.

The quantification of generated NH_3 was spectrophotometrically determined by the indophenol blue method. To ensure repeatability, each operating condition was measured at least three times.

The NH_3 yield rate was calculated via the equation as follows:

$$Y_{NH_3} = c_{NH_3} \times V/t \tag{1}$$

where Y_{NH_3} is the NH_3 yield rate, c_{NH_3} is the measured ammonia concentration, V is the volume of electrolyte, and t is the reaction time during electrocatalysis.

Ammonia faradaic efficiency was calculated according to the following equation:

$$\text{faradaic efficiency} = \frac{n \times V_{\text{catholyte}} \times c_{NH_3} \times F}{i \times t} \tag{2}$$

where i is the total current, n represents the number of electron transfers towards the formation of 1 mol of ammonia, which is 8 for nitrate reduction, $V_{\text{catholyte}}$ is the volume of catholyte (mL), c_{NH_3} represents the concentration of ammonia (mol L^{-1}), F is the Faraday constant (96485 C mol^{-1}), and t is the electrolysis time.

DFT calculation

The total energy and electronic structure calculations were performed by using the Vienna Ab-initio Simulation Package (VASP, Hafner, University of Vienna, Vienna, Austria), with the core electrons replaced by the projected augmented wave pseudo-potential. For the exchange–correlation energy, the Perdew–Burke–Ernzerhof (PBE) functional was used [18]. To simulate the reaction on the surface of the catalyst, the supercell was used with a vacuum layer of 15 Å, and a 3×3×1 Monkhorst–Pack grid was used for the *k*-point sampling of the Brillouin zone. The cutoff energy for the planewave basis set was set to 400 eV. The long-range dispersion interaction was described by the DFT-D3 method. The convergence criteria for the total energy and the Hellman–Feynman force are 10^{-5} eV and 0.02 eV $Å^{-1}$, respectively. The Gibbs free energy for the elemental steps was calculated by the following equation:

$$G = E + E_{\mathrm{ZPE}} - T\Delta S \tag{3}$$

E, E_{ZPE}, T, and S have been defined as the DFT total energy, zero-point energy, absolute temperature (298.15 K), and entropy, respectively. Vaspkit calculates the zero-point energy and entropy of the intermediates [19].

Results and discussion

Catalyst characterization

Electron microscopy was used to investigate the morphological and crystalline structure of the catalysts. Using high-resolution transmission electron microscopy (HRTEM), we observed lattice spacings of 0.213 nm for the Cu(111) facets (Fig. 1c) of the $Cu_{50}Ni_{50}$ catalysts due to the formation of the CuNi alloy phase, while lattice spacings of 0.183 nm were observed on pure Cu(111) facets (Fig. 1a) [16]. Compared with the dendritic morphologies observed from the Cu images, more catalyst clusters with diameters in the range of 50–100 nm were observed on the $Cu_{50}Ni_{50}$ samples as shown in Fig. 1b and d. The Cu-to-Ni ratio in the $Cu_{50}Ni_{50}$ catalyst, quantified by energy dispersive spectrometer (EDS) was 45:55. The corresponding X-ray EDS elemental mapping exhibits the homogeneous distribution of Cu and Ni throughout the whole structure.

Ar-plasma enhanced copper–nickel alloy catalysts

When the electrodeposition method was applied, we found that part of the generated metal catalysts could not completely adhere to the substrate. Thus, it was expected that the performance of copper-nickel may be deteriorated due to the large contact resistance caused by poor interaction between the substrate and the catalysts. To enhance the performance of the electrocatalysts, we applied radio-frequency non-thermal plasma to modify the substrate surface. We compared the performance of plasma treatment with three different types of feedstocks (air, argon, and nitrogen). Among them, the electrocatalyst with the Ar-plasma modified substrate outperformed the counterpart electrodes treated by Air and N_2 plasma as shown in Fig. 2a and b. For nitrate reduction, the current density of the Ar-plasma treated pure Cu catalyst reached 40 mA cm^{-2}, and the NH_3 yield rate was 1917 $\mu g_{NH_3} cm^{-2} h^{-1}$ in conventional H-type cell at −0.27 V vs. RHE, which was also much higher than most reported

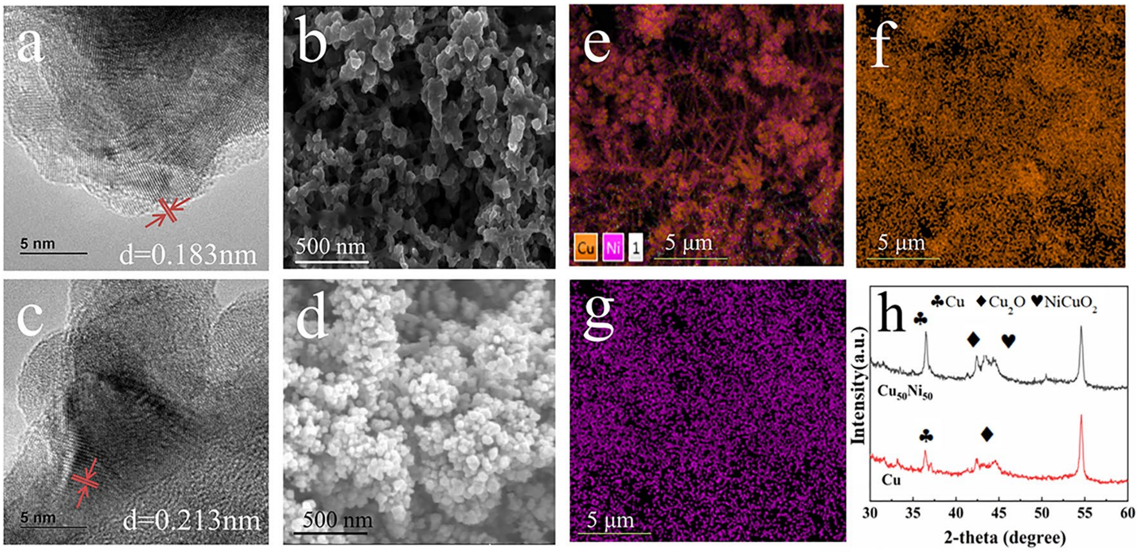

Fig. 1 Material characterization of copper-nickel alloy catalysts. (**a**), (**b**) HRTEM and SEM images of the pure Cu catalyst. (**c**), (**d**) HRTEM and SEM images of the $Cu_{50}Ni_{50}$ catalyst. The scale bars are 5 nm in (**a**) and (**c**), and 500 nm in (**b**) and (**d**). (**e**)–(**g**) EDS mapping of the $Cu_{50}Ni_{50}$ catalyst. (**h**) XRD patterns of the pure Cu catalyst and the $Cu_{50}Ni_{50}$ catalyst. *HRTEM* high-resolution transmission electron microscopy, *SEM* scanning electron microscopy, *EDS* energy dispersive spectrometer, *XRD* X-ray diffraction

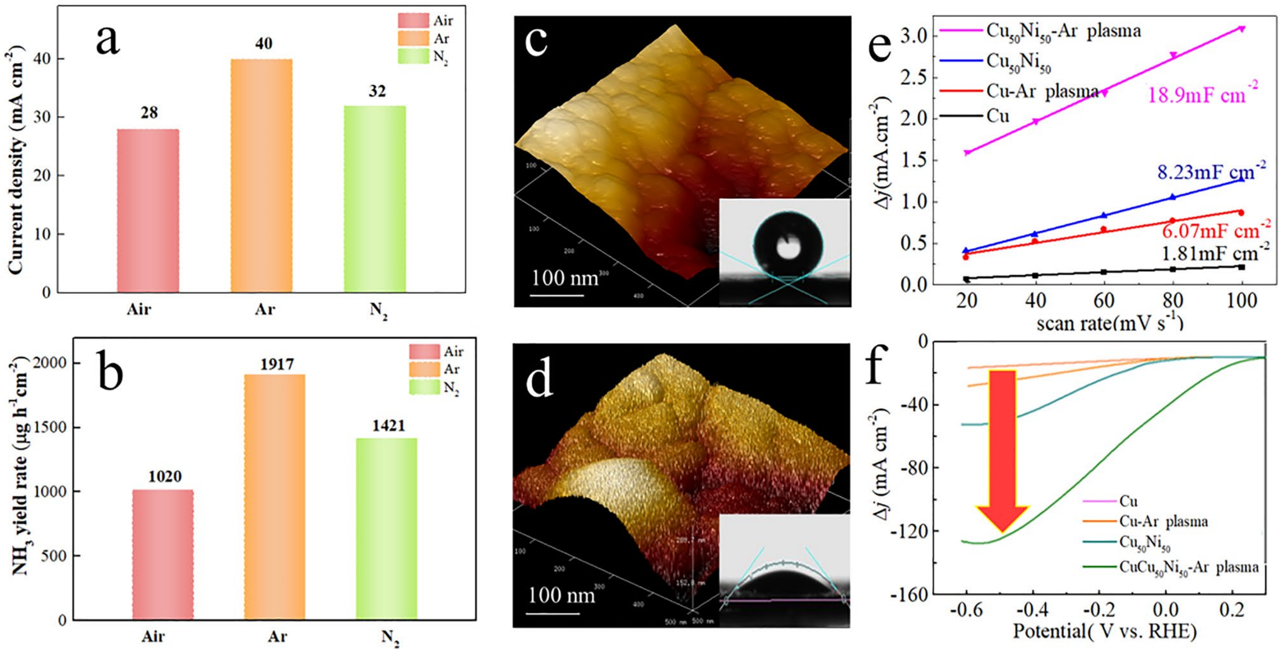

Fig. 2 (**a**) The current density and (**b**) the NH_3 yield rate using plasma modified pure Cu catalyst with different working gases (Air, Ar, and N_2) in 1 mol L^{-1} KOH + 0.1 mol L^{-1} KNO_3 electrolyte. Contact angle measurement and AFM images of carbon substrate without Ar-plasma treatment (**c**) and (**d**) with Ar-plasma treatment. (**e**) Comparison of ECSAs using different electrocatalysts (pure Cu, Ar-plasma modified Cu, $Cu_{50}Ni_{50}$ alloy, and Ar-plasma modified $Cu_{50}Ni_{50}$ alloy). (**f**) LSV curves of NO_3^- reduction on the different electrocatalysts (pure Cu, Ar-plasma modified Cu, $Cu_{50}Ni_{50}$ alloy, and Ar-plasma modified $Cu_{50}Ni_{50}$ alloy) in 1 mol L^{-1} KOH + 0.1 mol L^{-1} K NO_3^- electrolyte without iR compensation. *AFM* Atomic force microscopy, *ECSA* electrochemically active surface area, *LSV* linear sweep voltammetry, *RHE* reversible hydrogen electrode

electrocatalysts. It was indicated that Ar-plasma treatment has the best effect. Therefore, Ar-plasma has been applied for the subsequent experiments. Different from the air or N_2 plasma that are normally used to introduce oxygen- or nitrogen-containing radicals and components into the electrocatalyst, Ar-plasma is prone to change the physical roughness and hydrophobicity.

According to the contact angle measurement, the original carbon substrate was hydrophobic with a contact angle of 154.7°, while it became hydrophilic with a contact angle of 42.5° after Ar-plasma treatment (300 W) for 5 min. In Fig. 2c and d, the AFM images show that the plasma-treated carbon substrate is rougher with dense peaks and valleys compared to the relatively flat surface of the original carbon. On this basis, we speculated that the effect of plasma modification can be manifested in the etching of materials. Etching can remove weak boundaries, cause undulations, and increase the specific surface area. At the same time, the rough surface will decrease the contact angle, which is favorable for wetting and make it easier for the catalyst to adhere to the substrate. The unique morphology introduced by plasma could be explained as follows: the high-energy particles in the argon plasma include electrons, photons, excited particles, and free radicals. The free radicals are re-bonded to form a network cross-linked structure on the surface of the material [20, 21].

To gain further understanding of the plasma treatment role, we compared the electrochemically active surface area (ECSA) derived from the calculation of cyclic voltammetry curves. This result indicated that Ar-plasma treated electrocatalysts exhibited superior activity to the untreated counterparts as shown in Fig. 2e. For the CuNi alloy deposited on Ar-treated carbon substrates, the $ECSA_{Cu50Ni50}$ value is 18.9 mF cm^{-2}, which is two times higher than that without plasma modification. Even for the pure copper catalyst, the $ECSA_{Cu}$ with the Ar-treated substrate is 6.07 mF cm^{-2}, which is larger than that of the non-plasma-modified counterpart (only 1.81 mF cm^{-2}). This may be attributed to a change in roughness on the plasma-treated surface, enhancing the active sites for electrocatalytic reactions. The Ar-plasma-modified $Cu_{50}Ni_{50}$ alloy exhibits excellent performance in electrocatalytic NO_3^- reduction with ultra-low onset potential, outperforming all other electrocatalysts relying on linear sweep voltammetry (LSV) as shown in Fig. 2f. Under alkaline conditions, only a potential of 0.1 V is required to reach the current density of 50 mA cm^{-2} on $Cu_{50}Ni_{50}$ alloy with Ar-plasma modified substrate, and the current density of

$Cu_{50}Ni_{50}$ alloy can exceed 100 mA cm^{-2} at −0.3 V vs. RHE.

Electrocatalytic activity

To investigate the electrocatalytic activity of plasma-enhanced catalysts, a standard three-electrode system was applied. 0.1 mol L^{-1} NO_3^- was reduced in a typical H-type electrolytic cell separated by an anion exchange membrane. Colorimetric methods were adopted to determine the concentration of ammonia in the electrolytes. At the potential of −0.27 V vs. RHE, the faradaic efficiency of ammonia achieved the highest value of 98.1% along with 2610 $\mu g_{NH_3} cm^{-2}h^{-1}$ of NH_3 yield rate of the $Cu_{30}Ni_{70}$ alloy, while $Cu_{50}Ni_{50}$ alloy reached the highest NH_3 yield rate of 2725 $\mu g_{NH_3} cm^{-2}h^{-1}$. Furthermore, the Ar-plasma modified electrocatalyst exhibited a significant increase in NH_3 yield rate. The NH_3 yield rates of the treated $Cu_{30}Ni_{70}$ alloy, $Cu_{50}Ni_{50}$ alloy, and $Cu_{80}Ni_{20}$ alloy with plasma were 30.1%, 55.6%, and 50.1% higher than the corresponding untreated ones, respectively $Cu_{30}Ni_{70}$ (Fig. 3a). In addition, the NH_3 yield rate and the faradaic efficiency of NH_3 (aq) were evaluated in terms of different potentials (−0.07 V to −0.67 V vs. RHE). When the potential further decreased to −0.67 V vs. RHE, the NH_3 yield rate was increased as expected without sacrificing faradaic efficiency (Fig. 3b).

DFT calculations

DFT calculations were performed to explore the mechanism of the catalytic activity in CuNi alloys. Free energy changes for elementary reactions were calculated in the

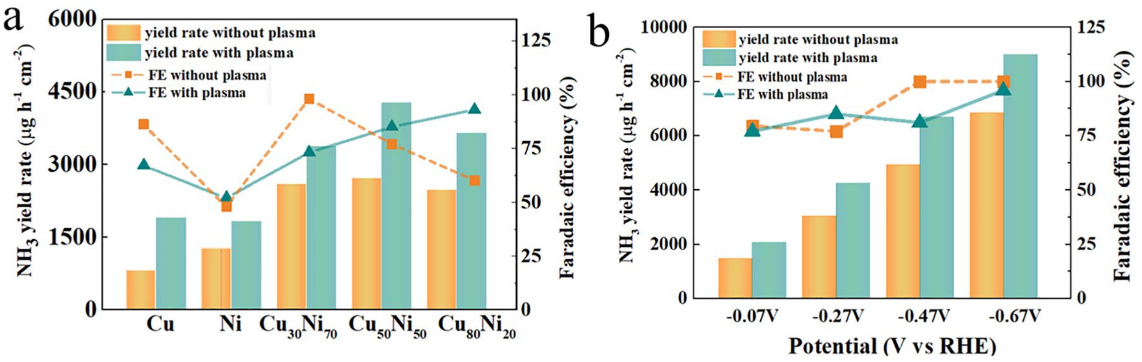

Fig. 3 Comparison of nitrate-to-NH_3 activity using $Cu_{50}Ni_{50}$ alloy before and after Ar-plasma treatment. (**a**) The effect of the Cu/Ni ratio on the NH_3 yield rate and faradaic efficiency at −0.27 V vs. RHE. (**b**) The effect of potential on the NH_3 yield rate and faradaic efficiency using the $Cu_{50}Ni_{50}$ catalyst

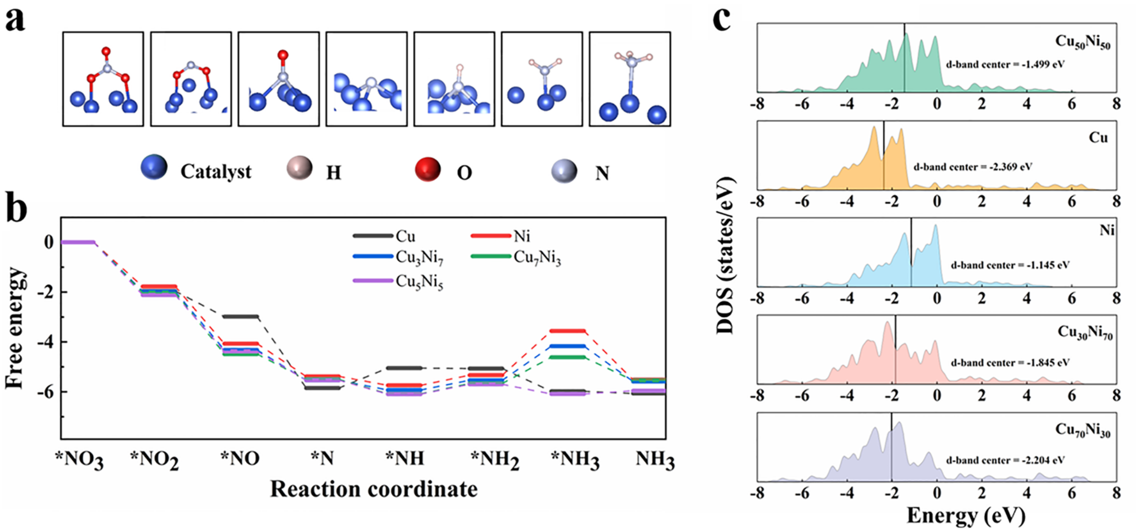

Fig. 4 DFT calculations of the nitrate-to-NH_3 reaction on CuNi alloy. (**a**) Reaction process of nitrate conversion to ammonia on the catalyst, the blue, pink, red, and grey spheres represent the Catalyst, H, O, and N atoms. (**b**) Free-energy diagrams of NO_3^- reduction to NH_3 on the surface of CuNi alloy. (**c**) The d-orbital density of states and d-band center of different catalysts. *DFT* density functional theory

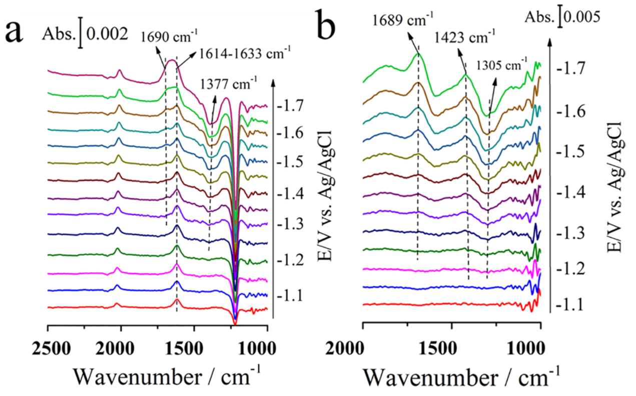

Fig. 5 **(a)** In situ internal reflection infrared spectroscopy (ATR-SEIRAS) and (**b**) in situ extrinsic reflectance infrared spectroscopy (IRAS) of the $Cu_{50}Ni_{50}$ alloy with Ar-plasma treatment via linear scanning in 1 mol L^{-1} KOH + 0.1 mol L^{-1} KNO_3 at different potentials (−0.9 V to −1.7 V vs. Ag/AgCl, displayed in different colors)

ammonia synthesis reaction from nitrate on the catalyst surface (Fig. 4b). Rate-determining steps (RDS) on Cu and Ni surfaces occur in the periods of *N to NH* and $*NH_2$ to $*NH_3$, respectively, and the high energy barrier hinders the rate of chemical reactions on the Cu or Ni catalysts. Through the combination of Cu and Ni, the energy barrier for the transition from *N to *NH is rapidly and effectively reduced, while the energy barrier for the transition from $*NH_2$ to $*NH_3$ is regulated. By adjusting the ratio of Cu:Ni, the energy barrier of $*NH_2$ hydrogenation reaches the lowest value when the ratio achieves 5:5, and the RDS energy current reduces to 0.234 eV, revealing the reason for the high yield rate and faradaic efficiency of the $Cu_{50}Ni_{50}$ catalyst. To further reveal the source of catalyst activity, PDOS (partial density of states) analysis and calculation of the d-band center were applied (Fig. 4c). The d-band center of the Cu catalyst (−2.369 eV) is significantly lower than that of the Ni catalyst (−1.145 eV), so adjusting the ratio of Cu:Ni doping is an effective method to enhance the non-uniform charge distribution and optimize the center position of the d-band. The d-band center of $Cu_{50}Ni_{50}$ is significantly closer to the Fermi level than other catalysts (−1.449 eV compared to −1.845 eV and −2.204 eV). The high energy level of the d-band center increases the adsorption capacity of NO_3^-RR intermediates to the surface of the catalyst, which theoretically improves the NO_3^-RR performance of the $Cu_{50}Ni_{50}$ alloy [22, 23].

Transient FTIR experiments were carried out to capture the adsorbed intermediates to investigate the effect of substrate-electrocatalyst interface modification by Ar-plasma. In Fig. 5a, negative bands at about 1250 cm^{-1} corresponding to the consumption of NO_3^- were observed during nitrate conversion using the $Cu_{50}Ni_{50}$ alloy. With the decrease in potential from −0.9 V to −1.7 V vs. Ag/AgCl, the large consumption of NH_3 was observed together with the observation of the NO band at about 1377 cm^{-1} and the NH_3 band at about 1690 cm^{-1}. For in situ extrinsic reflectance infrared spectroscopy in Fig. 5b, two obvious bands assigned to NO (about 1305 cm^{-1}) and $NH_{x,ad}$ (about 1423 cm^{-1}) were observed, which implied that the intermediates of NO* was key for nitrate conversion and were prone to be formed after plasma treatment. This is consistent with the calculation results [24–26].

Conclusions

In this article, we synthesized an effective bimetallic catalyst that can be used for the electrocatalytic reduction of nitrate and demonstrated that substrate modification by Ar-plasma can improve the performance of electrocatalysts. We found that plasma-modified substrate can change the hydrophobicity of the substrate and strengthen the connection between the catalysts and the substrate. In addition, the current density, normalized to the ECSA, was significantly improved after the substrate was modified by Ar-plasma, thereby improving the electrochemical performance of the reaction. The pure Cu catalyst was synthesized first and exhibited superior performance for nitrate reduction to ammonia with faradaic efficiency (73.2%), and NH_3 yield rate (2060 $\mu g_{NH_3} cm^{-2} h^{-1}$) at −1.3 V vs. SCE. By replacing 50% Cu with Ni, the NO_3^-RR-to-NH_3 performance was enhanced significantly. This includes a high NH_3 yield rate of 2725 $\mu g_{NH_3} cm^{-2} h^{-1}$ and 77.9% faradaic efficiency. DFT calculations verify that $Cu_{50}Ni_{50}$ catalyst has the smallest rate-determining step (0.234 eV) and the closest center position of the d-band to the Fermi level (−1.449 eV), which is the source of the high activity of $Cu_{50}Ni_{50}$. Furthermore, in situ FTIR spectra confirmed the formation of NO^* and the intermediate of NO_2^- during the electroreduction of nitrate. This work offers a facile strategy to synthesize efficient electrocatalysts for ammonia synthesis from nitrate reduction.

Acknowledgements This work is supported by the National Natural Science Foundation of China (No. 51976191) and the State Key Laboratory of Clean Energy Utilization (No. ZJUCEU2021003), Ecological civilization project, Zhejiang University and the Fundamental Research Funds for the Central Universities.

Declarations

Conflict of interest The authors declare that they have no conflict of interest.

References

1. Foster, S.L., Perez-Bakovic, S.I., Duda, R.D., et al. 2018. Catalysts for nitrogen reduction to ammonia. *Nature Catalysis* 1: 490–500.
2. Lee, H.K., Koh, C.S.L., Lee, Y.H., et al. 2018. Favoring the unfavored: selective electrochemical nitrogen fixation using a reticular chemistry approach. *Science Advances* 4: e3208.
3. Shipman, M.A., and Symes, M.D. 2017. Recent progress towards the electrosynthesis of ammonia from sustainable resources. *Catalysis Today* 286: 57–68.
4. Martín, A.J., and Pérez-Ramírez, J. 2019. Heading to distributed electrocatalytic conversion of small abundant molecules into fuels, chemicals, and fertilizers. *Joule* 3: 2602–2621.
5. Zi, X., Wan, J., Yang, X., et al. 2021. Vacancy-rich 1T-MoS_2 monolayer confined to MoO_3 matrix: an interface-engineered hybrid for efficiently electrocatalytic conversion of nitrogen to ammonia. *Applied Catalysis B: Environmental* 286: 119870.
6. Wang, C., Gu, L.-L., Qiu, S.-Y., et al. 2021. Modulating $CoFe_2O_4$ nanocube with oxygen vacancy and carbon wrapper towards enhanced electrocatalytic nitrogen reduction to ammonia. *Applied Catalysis B: Environmental* 297: 120452.
7. Davidson, E.A., David, M.B., Galloway, J.N., et al. 2012. Excess nitrogen in the US environment: trends, risks, and solutions. *Issues in Ecology* 15: 1–16.
8. Rosca, V., Duca, M., de Groot, M.T., et al. 2009. Nitrogen cycle electrocatalysis. *Chemical Reviews* 109: 2209–2244.
9. Seraj, S., Kunal, P., Li, H., et al. 2017. PdAu alloy nanoparticle catalysts: Effective candidates for nitrite reduction in water. *ACS Catalysis* 7: 3268–3276.
10. Wang, D., He, N., Xiao, L., et al. 2021. Coupling electrocatalytic nitric oxide oxidation over carbon cloth with hydrogen evolution reaction for nitrate synthesis. *Angewandte Chemie International Edition* 46: 24605–24611.
11. Chen, J.G., Crooks, R.M., Seefeldt, L.C., et al. 2018. Beyond fossil fuel-driven nitrogen transformations. *Science* 360: eaar6611.
12. Hawtof, R., Ghosh, S., Guarr, E., et al. 2019. Catalyst-free, highly selective synthesis of ammonia from nitrogen and water by a plasma electrolytic system. *Science Advances* 5: eaat5778.
13. Singh, A.R., Rohr, B.A., Schwalbe, J.A., et al. 2017. Electrochemical ammonia synthesis-the selectivity challenge. *ACS Catalysis* 7: 706–709.
14. Dima, G.E., de Vooys, A.C.A., and Koper, M.T.M. 2003. Electrocatalytic reduction of nitrate at low concentration on coinage and transition-metal electrodes in acid solutions. *Journal of Electroanalytical Chemistry* 554: 15–23.
15. McEnaney, J.M., Blair, S.J., Nielander, A.C., et al. 2020. Electrolyte engineering for efficient electrochemical nitrate reduction to ammonia on a titanium electrode. *ACS Sustainable Chemistry & Engineering*. 8: 2672–2681.
16. Wang, Y., Aoni, X., Wang, Z., et al. 2020. Enhanced nitrate-to-ammonia activity on copper-nickel alloys via tuning of intermediate adsorption. *Journal of the American Chemical Society* 142: 5702–5708.
17. Fu, X., Zhao, X., Hu, X., et al. 2020. Alternative route for electrochemical ammonia synthesis by reduction of nitrate on copper nanosheets. *Applied Materials Today* 19: 100620.
18. Perdew, J.P., Burke, K., and Ernzerhof, M. 1996. Generalized gradient approximation made simple. *Physical Review Letters* 77: 3865.
19. Wang, V., Xu, N., Liu, J.C., et al. 2021. VASPKIT: A user-friendly interface facilitating high-throughput computing and analysis using VASP code. *Computer Physics Communications*. 267: 108033.
20. Dumitrascu, N., Topala, I., and Popa, C. 2005. Dielectric barrier discharge technique in improving the wettability and adhesion properties of polymer surfaces. *IEEE Transactions on Plasma Science* 33: 1710–1714.
21. Wu, A., Yang, J., Xu, B., et al. 2021. Direct ammonia synthesis from the air via gliding arc plasma integrated with single atom electrocatalysis. *Applied Catalysis B: Environmental* 299: 120667.
22. Niu, H., Zhang, Z., Wang, X., et al. 2021. Theoretical insights into the mechanism of selective nitrate-to-ammonia electroreduction on single-atom catalysts. *Advanced Functional Materials* 31: 2008533.
23. Nørskov, J.K., Bligaard, T., Logadottir, A., et al. 2005. Trends in the exchange current for hydrogen evolution. *Journal of the Electrochemical Society* 24: 23–26.
24. Figueiredo, M.C., Solla-Gullón, J., Vidal-Iglesias, F.J., et al. 2013. Nitrate reduction at Pt(100) single crystals and preferentially oriented nanoparticles in neutral media. *Catalysis Today* 202: 2–11.
25. Pérez-Gallent, E., Figueiredo, M.C., and Katsounaros, I. 2017. Electrocatalytic reduction of Nitrate on Copper single crystals in acidic and alkaline solutions. *Electrochimica Acta* 227: 77–84.
26. Da Cunha, M.C.P.M., de Souza, J.P.I., and Nart, F.C. 2000. Reaction pathways for reduction of nitrate ions on platinum, rhodium, and platinum-rhodium alloy electrodes. *Langmuir* 16: 771–777.